Environ. Sci. Technol. **2010,** *44,* 5570–5574

New Type of $BiPO_4$ Oxy-Acid Salt Photocatalyst with High Photocatalytic Activity on Degradation of Dye

CHENGSI PAN AND YONGFA ZHU*

Department of Chemistry, Tsinghua University, Beijing 100084, P.R. China

Received April 16, 2010. Revised manuscript received June 11, 2010. Accepted June 16, 2010.

A high photocatalytic $BiPO_4$ with a novel nonmetal oxy acid structure is synthesized by a hydrothermal method. $BiPO_4$ photocatalyst has an optical indirect band gap of 3.85 eV. In a comparison of $BiPO_4$ with that of TiO_2 (P25, Degussa), it is found that the photocatalytic activity of $BiPO_4$ is twice that of TiO_2 (P25, Degussa) for the degradation of methylene blue (MB) dye, while the BET surface of $BiPO_4$ is just one tenth of that of P25. Both the high position of the valence band and the high separation efficiency of electron−hole pairs result in the high photocatalytic activity. The inductive effect of PO_4^{3-} helps the e^-/h^+ separation, which plays an important role in its excellent photocatalytic activity. It may extend to the synthesis of other inorganic nonmetal salts of oxy photocatalysts with suitable band gap and high activity for the environmental purification of organic pollutants in aqueous solution.

Introduction

The decolorization and mineralization of dyes from textile wastewater is a pertinent issue, and currently there is no simple and economical treatment that can effectively remove dyes (*1*). In addition, data show that 10% to 15% manufactured dyes are lost in wastewater (*2*). Although some methods cause rapid decolorization, the breakdown products may be more hazardous than the original dyes. Photocatalytic technology attracts much attention due to the application on completely removing environmental pollutants in wastewater and effluents. Unlike the conventional biodegradable or activated carbon adsorption method, photocatalysis especially for TiO_2-based photocatalytic technology offers a powerful oxidation in the treatment of bioresistant organic contaminants such as dye wastewater by converting them into CO_2 (*3*). Nevertheless, the photocatalytic activity of TiO_2 is not high enough to meet the need of industrial usages due to a rapid recombination between photogenerated electrons and holes, which makes high running costs.

Currently, some new photocatalysts, mostly focused on metal oxide and composite metal oxide semiconductors, have been tested in order to overcome the drawbacks of TiO_2 (*4*−*7*). In spite of the extensive research on the new photocatalytic systems in the past, efficient photocatalysts with high photocatalytic activity (compared to the commercial TiO_2, P25), good stability, and low cost are still rare. On the other hand, the anions in the nonmetal oxy-acid salts doped TiO_2, like PO_4^{3-}, SO_4^{2-} have been reported to be effective to enhance the photocatalytic activity due to the strong bonding ability with H_2O, the high negative energy to draw the hole to the interface by the electrostatic force, and the chemical-redox inertness to the photogenerated electrons and holes (*8, 9*). Besides that, anions in the nonmetal oxy-acid salts are inexpensive and almost nontoxic. Concerning the benefits of the anions in the nonmetal oxy-acid salts mentioned above, their salts may also have excellent activity in the photocatalytic reaction. However, few studies on the nonmetal salts of oxy-acid photocatalysts have been reported, and the main oxidative specie (·OH, or h^+) in the nonmetal salt of an oxy acid photocatalyst is still not clear.

Herein we report a new type inorganic nonmetal salt of oxy-acid photocatalyst, $BiPO_4$, which exhibits a more superior photocatalytic activity than that of P25 on dye degradation. Bismuth salt photocatalysts usually have a narrow band gap due to the rise of valence band caused by Bi 6s and O 2p antibonding states, like $BiVO_4$ and $CaBi_2O_4$ (*10, 11*). Also, these bismuth salts have promising photocatalytic efficiency. For example, Bi_2WO_6, reported by other groups and us, exhibited superior photocatalytic activity for the degradation of rhodamine B (RhB) and methylene blue (MB) under visible light irradiation (*12*−*16*). $BiPO_4$, as one of them, finds applications in catalysis and ion sensing and can be used for separating radioactive elements (*17*−*19*). To our best knowledge, there is no report on the photocatalytic activity of $BiPO_4$. In this paper, the $BiPO_4$ was synthesized by a hydrothermal method. It is a well established technique to synthesis nanosized metal oxide and composite metal oxide semiconductors (*20, 21*). MB was chosen as to simulate a general dye pollutant to evaluate its photocatalytic activity in aqueous medium under UV lamp, and a comparison on $BiPO_4$ and TiO_2 (P25, Degussa) is presented. PO_4^{3-}, possessing a large negative charge, is postulated to help the e^-/h^+ separation, which plays an important role in its excellent photocatalytic activity. In addition, this property may extend to the synthesis of other nonmetal salts of oxy-acid photocatalysts with suitable band gap and high activity for the environmental purification of organic pollutants in aqueous solution.

Experimental Section

Synthesis. $BiPO_4$ was synthesized through a hydrothermal process. All chemicals used were analytic grade reagents without further purification. Three mmol of $Bi(NO_3)_3$•$6H_2O$ and equal molar Na_3PO_4•$12H_2O$ were put into a beaker. Then, 30 mL of distilled water was added to the beaker and magnetically stirred to form a homogeneous solution at room temperature. The pH was adjusted to 1 by the addition of concentrated HNO_3. The resulting precursor suspension was transferred into a Teflon-lined stainless steel autoclave and maintained at 180 °C for 72 h. The products were washed several times with distilled water and dried at 80 °C for 24 h, subsequently.

Characterization. UV−vis diffuse reflectance spectra (DRS) of the samples were measured by using Hitachi U-3010 UV−vis spectrophotometer. The Brunauer−Emmett−Teller (BET) specific surface area of the sample was characterized by nitrogen adsorption at 77 K with Micromeritics 3020. Total organic carbon analyzer (TOC-V_{wp}, Shimadzu, Japan) was employed for mineralization degree analysis of MB solutions.

Photocatalytic Evaluation. Photocatalytic activities of $BiPO_4$ (or P25) were evaluated by degradation of methylene blue (MB) under ultraviolet light irradiation of an 11 W low-pressure lamp with 254 nm. The average light intensity was 1.5 mW/cm^2. The radiant flux was measured with a power

* Corresponding author phone: +86-10-62783586; fax: +86-10-62787601; e-mail: zhuyf@mail.tsinghua.edu.cn.

10.1021/es101223n
Published on Web 06/25/2010

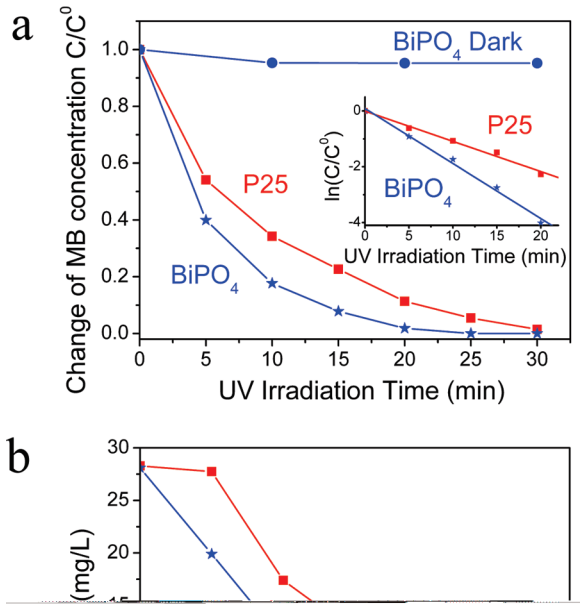

FIGURE 1. (a) Photocatalytic degradation curves of MB for $BiPO_4$ and P25 (Degussa, TiO_2), respectively. Photocatalysts (both $BiPO_4$ and P25), 0.5 g/L; MB concentration, 10^{-5} mol/L. (b) Changes in TOC during the course of photocatalytic degradation of MB in the presence of $BiPO_4$ and P25, respectively.

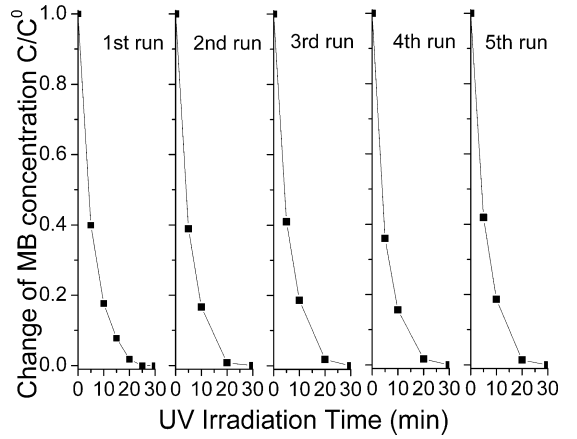

FIGURE 2. Cycling runs in the photocatalytic degradation of MB in the presence of $BiPO_4$.

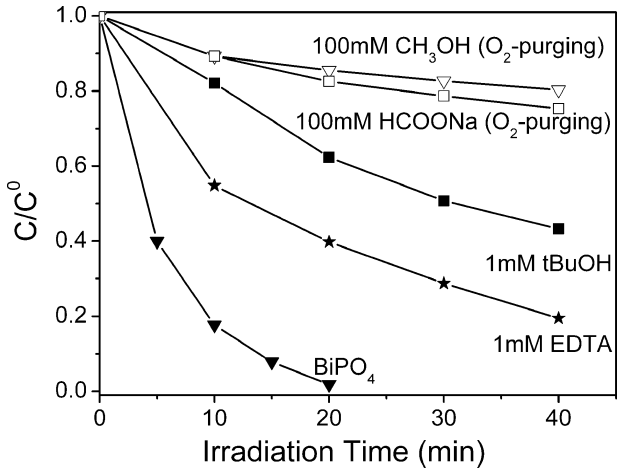

FIGURE 3. Plots of photogenerated carriers trapping in the system of photodegradation of MB on $BiPO_4$.

meter from the Institute of Electric Light Source (Beijing). MB solutions (200 mL, 10^{-5} mol L^{-1}) containing 0.100 g of $BiPO_4$ (or P25) were put in a glass beaker. Before the light was turned on, the solution was first ultrasonicated for 10 min and then stirred for 10 min to ensure equilibrium between the catalysts. Three milliliters of the sample solution was taken at given time intervals and separated through centrifugation (4000 rpm, 10 min). The supernatants were analyzed by recording variations of MB at the absorption band maximum (664 nm) in the UV−vis spectra using a U-3010 spectrophotometer (Hitachi).

Result and Discussion

Photocatalytic Property of $BiPO_4$ and the Mineralized Degree. The MB degradation catalyzed by $BiPO_4$ was investigated. As a comparison, the MB photodegraded by TiO_2 (P25) was also performed. The MB concentrations versus the reaction time in both the $BiPO_4$ and TiO_2 (P25) systems are plotted in Figure 1a, respectively. MB is completely photodegraded catalyzed by $BiPO_4$ in 20 min, while 15% MB remains in the reaction by TiO_2 (P25). MB photolysis without the photocatalyst and the dark reaction between the dye and catalysts (Figure 1a) can almost be neglected. Therefore, $BiPO_4$ has better photocatalytic activity in MB degradation reaction than TiO_2 (P25). In addition, due to pseudo-first-order kinetics of MB photodegradation on $BiPO_4$, the experimental data obviously show the apparent rate constant k is 0.101 min^{-1} and 0.197 min^{-1} for P25 and $BiPO_4$, respectively (Figure 1 inset). In other words, the photocatalytic activity of $BiPO_4$ is twice that of P25.

To further investigate the activity of $BiPO_4$, the TOC experiment was performed, shown in Figure 1b. The result shows that the mineralization yield of $BiPO_4$ reaches a value of 84.4% after 25 min of irradiation, while that of P25 is 74.2% after 30 min of irradiation. This rate of TOC reduction of $BiPO_4$ is slower than that of the degradation of dye, which is nearly 100% discoloration for MB in 25 min as shown Figure 1a. It is well-known that the mineralization of the dye goes through two steps: the ring cleavage and subsequently the oxidation of the fragments (*22*). In our experiment, the decreasing TOC rate of $BiPO_4$ exhibited two different behaviors before and after 15 min of irradiation, respectively, indicating that MB is first ring cleavage and then converted into CO_2.

Also, after five recycles for the photodegradation of MB, the catalyst did not exhibit any significant loss of activity, as shown in Figure 2, confirming $BiPO_4$ is not photocorroded during the photocatalytic oxidation of the pollutant molecules. To test the stability of the sample during the photocatalytic process, we analyzed it before and at the end of the reaction by XRD (Supporting Information Figure S1). After reaction, no obvious change has been observed, indicating its good stability.

The radicals and holes trapping experiments were designed to elucidate the photocatalytic degradation process of $BiPO_4$. As shown in Figure 3, under irradiation the photodegradation of MB is slightly suppressed by the addition of a hole scavenger, EDTA (*23*), while it is obviously inhibited when a hydroxyl radical scavenger, tBuOH, was added (*23*). This indicates that hydroxyl radicals are the main active species that can oxidize the adsorbed organic pollutants, which is also reported as the dominantly active ones in TiO_2 (*3*). Meanwhile, $HO_2\bullet/O_2^-\bullet$ may also serve as active species

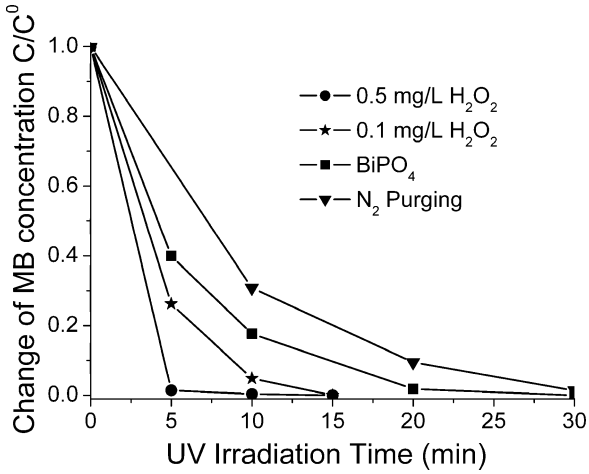

FIGURE 4. Effect of H_2O_2 and N_2 on the photocatalytic degradation of MB in the presence of $BiPO_4$.

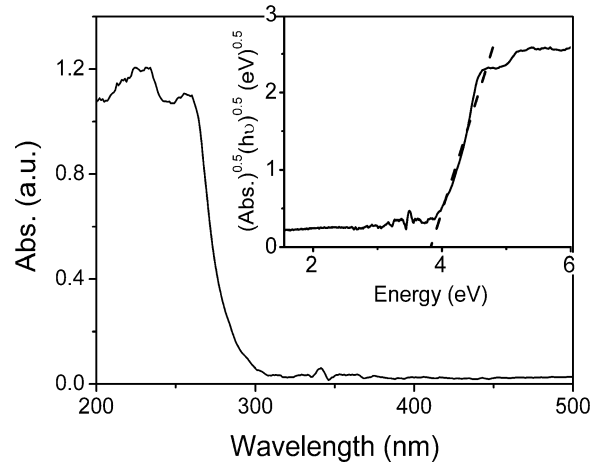

FIGURE 5. UV−vis diffuse reflectance of $BiPO_4$; the inset in the upper right is the absorption$^{1/2}$ versus energy curve.

in many reactions. In the presence of 100 mM methanol or formate ($k(CH_3OH + OH\bullet) = 9.7 \times 10^8\ M^{-1}\ s^{-1}$, $k(HCOO^- + OH\bullet) = 3.2 \times 10^9\ M^{-1}\ s^{-1}$ (*24*)), the majority of OH radicals can be converted into $HO_2\bullet/O_2^-\bullet$ (reactions 1−4) (*25*). Accordingly, if $HO_2\bullet/O_2^-\bullet$ is an effective oxidant of MB, the degradation would be greatly increased by methanol or formate, which is inconsistent with the results shown in Figure 3. It also suggests that hydroxyl radicals play an important role in the $BiPO_4$ photocatalytic system.

$$\cdot OH + CH_3OH \rightarrow H_2O + \cdot CH_2OH \quad (1)$$

$$\cdot CH_2OH + O_2 \rightarrow HCHO + HO_2\cdot \quad (2)$$

$$\cdot OH + HCOO^- \rightarrow H_2O + CO_{2^-}\cdot \quad (3)$$

$$CO_{2^-}\cdot + O_2 \rightarrow CO_2 + O_{2^-}\cdot \quad (4)$$

This •OH can be formed through the hole oxidation of OH^- or the reduction of O_2 (reactions 5−7). The former route is controlled by the potential of the holes in the valence band (discussed below). Meanwhile, H_2O_2 is a key intermediate product for the latter route, which can easily break down and generate the reactive •OH radicals. The H_2O_2 concentration during reaction is detected (Table S1). And also, the photocatalytic degradation of MB is significantly improved by the presence of H_2O_2 as shown in Figure 4, indicating that the photogenerated electron-induced multistep reduction of O_2 is one part source of •OH radicals. N_2 is also a good detective molecular to make certain the effect of O_2, shown in Figure 4. Under the anoxic suspension, the photodegraded rate of MB is largely prohibited; indicating O_2 is a key factor in the photoreduction process that produces the super oxide and hydroxyl radicals.

$$OH^- + h^+ \rightarrow \cdot OH \quad (5)$$

$$O_2 + 2H^+ + 2e^- \rightarrow H_2O_2 \quad (6)$$

$$H_2O_2 + e^- \rightarrow \cdot OH + OH^- \quad (7)$$

Structure and Optical Properties of $BiPO_4$. The structure of $BiPO_4$ was examined by XRD, as shown in Supporting Information Figure S1. The result shows that all of the diffraction peaks can be indexed to the pure monoclinic phase of $BiPO_4$ (JPCDS 80-0209). The width of the three highest peaks is all less than 0.2°, and this narrow broadening of the peaks implies a high purity and crystalline. The size and morphology of the products were obtained by SEM, TEM, and HRTEM (Figure S2a,b,c), which show that the obtained samples exhibit 1D nanostructure. The as-prepared nanorod is 400 ± 100 nm in length and 80 ± 20 nm in width. The HRTEM (Figure S2d) image shows that the nanorods grow along the [100] direction.

Reflectance spectra of $BiPO_4$ are shown in Figure 5. The absorption edge of $BiPO_4$ occurs at about 322 nm, and the band gap energy is estimated to be 3.85 eV, which is larger than that of TiO_2 (3.23 eV). In semiconductors, the square of absorption coefficient is linear with energy for direct optical transitions in the absorption edge region; whereas the square root of absorption coefficient is linear with energy for indirect transitions (*26*). Data plots of absorption$^{1/2}$ versus energy in the absorption edge region are shown in the inset of Figure 5, which is nearly linear. This feature suggests that the absorption edge of $BiPO_4$ is caused by indirect transitions.

Photocatalytic Mechanism. The photocatalytic activity is governed by various factors such as surface area, the band gap, the oxidation potential of photogenerated holes, and the separation efficiency of photogenerated electrons and holes (*3, 13*). In the $BiPO_4$ system, the BET surface area is only 3 m^2/g, much less than that of P25 (50 m^2/g). While the band gap is larger than that of TiO_2, which means less UV-light can be harvested.

On the other hand, the flat band potential is −0.63 V (vs Ag/AgCl), which is 80 mV higher than that of anatase TiO_2 (−0.55 V vs Ag/AgCl (*27*)) (Supporting Information Figure S3). This negative shift will be in relation to the increase of the redox potential of the conduction band and, in somewhere, raise the position of the valence band and make the oxidation potential of holes not as high as that in other wide-gap photocatalysts. Furthermore, we can calculate its conduction and valence band positions through the following equation: $E_{VB} = X - Ee + 0.5Eg$ (*28*), where X is the Mulliken's electronegativities, Ee is the energy of free electrons on the hydrogen scale (≈4.5 eV), and Eg is the band gap. The E_{VB} is estimated to be 3.2 V, which is 0.3 V higher than that of TiO_2 (2.9 V (*28*)), which may facilitate for the holes generated to react with OH^-, producing active •OH radicals. This may be one reason for the high activity. However, this driving force due to the difference between the potential of the valence band of TiO_2 and $BiPO_4$ is not large enough to completely explain why the activity of $BiPO_4$ is higher than that of P25. In other wide-gap photocatalysts such as $In(OH)_3$ (E_{VB} = 4.2 eV) and $CaSb_2O_5(OH)_2$ (E_{VB} = 4.1 eV) (*29, 30*) with good photocatalytic performance, the difference is much larger. So it is reasonable to believe that there are some more important reasons for its high activity, which may be the separation efficiency of electron and hole pairs according to the classic photocatalytic theory.

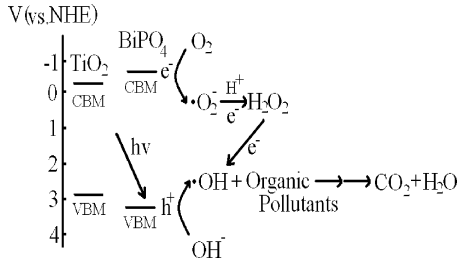

FIGURE 6. Proposed mechanism of photocatalytic degradation of organic pollutants on $BiPO_4$.

The separation and transfer of electron and hole pairs can be indicated by electrochemical impedance spectroscopy (EIS) (*31*). As shown in Figure S4, the diameter of the $BiPO_4$ semicircle tends to obviously decrease under UV illumination due to the large increase of the charge transfer and the separation of the e^-/h^+ pairs. Compared to P25, the diameter of the $BiPO_4$ semicircle is also smaller under UV illumination, which implies a better photocatalytic activity than that of P25. To obtain more detailed information, an equivalent circuit can be designed for $BiPO_4$ (Figure S4 inset), which is also proved essentially on TiO_2 nanorods (*32*). The results are shown in Figure S4 and Table S2. The theoretical curves are in good agreement with the experimental impedance data, thereby validating the proposed equivalent circuit in this system. The variation of electrolyte resistance *R* reflects the separation and transfer of electron and hole pairs (*32*). The difference in *R* in the dark and under UV is a 5-fold difference for P25 and a 7-fold difference for $BiPO_4$, which indicates a reduction in the probability of the recombination of the e^-/h^+ pairs and an increase of the charge transfer of the latter. This is the main reason for the high activity of $BiPO_4$.

In a word, not only the high potential of photogenerated holes in the valence band but also the high separation efficiency of electron−hole pairs benefits for the production of active •OH radicals. These radicals can directly destroy the ring structure of the dye molecular and then convert it into CO_2 by either H atom abstraction, direct electron transfer, or insertion. On the basis of the discussion above, a possible mechanism for the photodegradation of organic pollutants over $BiPO_4$ is proposed in Figure 6.

Effect of PO_4^{3-} Ions on the Photocatalyst of $BiPO_4$. According to the above discussion, the high photocatalytic performance of $BiPO_4$ is mainly due to the high separation efficiency of electron and hole pairs. This high separation efficiency should be closely attributed to a specific nonmetal salt of the oxy-acid structure of $BiPO_4$. It is noteworthy that PO_4^{3-} ions have a large negative charge which maintains a large dipole in the $BiPO_4$, which prefers the photogenerated charge separation. This effect is called an inductive effect described as the action of one group to affect electrostatically the electron distribution in another group. In the previous work, Inoue et al. show that $CaIn_2O_4$ and $SrIn_2O_4$ with a large dipole moment have a remarkable photocatalytic activity, while the negligible activity has been found on $LiInO_2$ and $NaInO_2$ with low local polarization (*33*). This effect may also be seen in other phosphate salts like $LiFePO_4$ or $LiCoPO_4$, in which the large negative charge of PO_4^{3-} ions is regarded to stabilize the Fe^{2+}/Fe^{3+}, and, thus, $LiFePO_4$ becomes a popular positive electrode material for lithium batteries (*34*). To understand this feature deeply, the projections of the wave function for the total electron density, LUMO, and HOMO through a (001) plane containing both Bi and P atoms were shown in Supporting Information Figure S5. The projections of the HOMO and LUMO show that one photon excites one electron from O2p states to Bi 6p states. Meanwhile PO_4^{3-}, possessing a large electron cloud overlapping (total electron density, Supporting Information Figure S5a), prefers to attract holes and repel electrons, which helps the e^-/h^+ separation. On the other hand, due to the strong P−O covalence, PO_4^{3-} ions are difficult to form oxygen vacancies which are considered as the recombination centers in TiO_2 or other metal oxide and composite metal oxide photocatalysts (*3, 4*). In addition, PO_4^{3-} ions on the surface of $BiPO_4$ may also play the same part as they do in the TiO_2 surface, such as the strong bonding ability with H_2O. These benefits of PO_4^{3-} ions in the structure may result in its photocatalytic superiority.

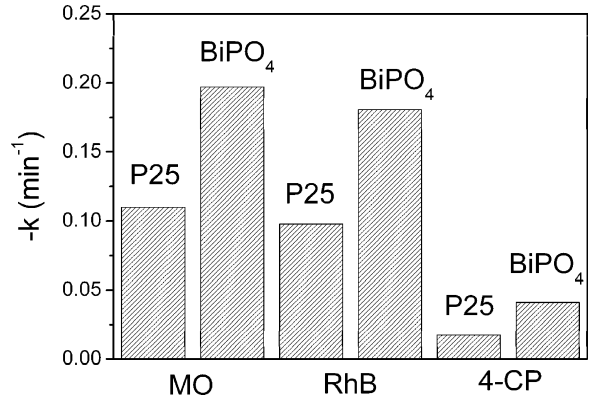

FIGURE 7. Selectivity on the photocatalytic degradation of MO, RhB, and 4-CP in the presence of $BiPO_4$. The concentration variety of the above three pollutants is determinned by the absorption peak at 460 nm, 554 nm, and 225 nm, respectively.

Furthermore, this property may be common in other nonmetal salts of oxy-acid. In any case, this work is an outstanding example of a nonmetal salt of oxy-acid photocatalyst that shows such high reactivity, much higher than those for most of the previously reported materials. In this regard, it is an important discovery for the synthesis of other nonmetal salts of oxy-acid photocatalysts with suitable band gap and much higher activity than TiO_2. In addition, the cost of $BiPO_4$ is 0.23 $/g. while P25 is 1.21 $/g. $BiPO_4$ is only one-sixth of that of P25. So we believe that the nonmetal salts of oxy-acid are efficient for the environmental purification of organic pollutants in aqueous solution.

Besides that, it is well-known that hydroxyl radicals are almost nonselective, and, that is, they will directly react with various organic pollutants due to its high redox potential of 2.7 V vs NHE. In fact, the photodegradation of other pollutants on $BiPO_4$ (Figure 7) confirms this conclusion. It shows that the degradation activity of $BiPO_4$ on anionic dye (rhodamine B (RhB)), cationic dye (methyl orange (MO)), or other neutral benzene ring compounds (4-chlorophenol (4-CP)) is obviously higher than that of P25, which suggests that the high activity of $BiPO_4$ is not due to the special combination of the catalysts to some specific substrates but due to the hydroxyl radical reactions. Therefore, the high photocatalytic activity of $BiPO_4$ may be general and essential for environmental application.

Acknowledgments

This work was partly supported by the National Natural Science Foundation of China (20925725 and 50972070) and National Basic Research Program of China (2007CB613303).

Supporting Information Available

Detailed experimental procedures, theoretical calculation, and additional figures. This material is available free of charge via Internet at http://pubs.acs.org.

Literature Cited

(1) dos Santos, A. B.; Cervantes, F. J.; van Lier, J. B. Review Paper on Current Technologies for Decolourisation of Textile Wastewaters: Perspectives for Anaerobic Biotechnology. *Bioresour. Technol.* **2007**, *98*, 2369–2385.

(2) Zollinger, H. *Color Chemistry - Syntheses, Properties and Applications of Organic Dyes and Pigments*; VCH Publishers: New York, 1987.

(3) Hoffmann, M. R.; Martin, S. T.; Choi, W.; Bahnemann, D. W. Environmental Applications of Semiconductor Photocatalysis. *Chem. Rev.* **1995**, *95*, 69–96.

(4) Kudo, A.; Miseki, Y. Heterogeneous Photocatalyst Materials for Water Splitting. *Chem. Soc. Rev.* **2009**, *38*, 253–278.

(5) Ding, Y.; Wan, Y.; Min, Y. L.; Zhang, W.; Yu, S. H. General Synthesis and Phase Control of Metal Molybdate Hydrates $MMoO_4 \cdot nH_2O$ (M=Co, Ni, Mn, n = 0, 3/4, 1) Nano/Microcrystals by a Hydrothermal Approach: Magnetic, Photocatalytic, and Electrochemical Properties. *Inorg. Chem.* **2008**, *47*, 7813–7823.

(6) Zhou, Y. X.; Yao, H. B.; Zhang, Q.; Gong, J. Y.; Liu, S. J.; Yu, S. H. Hierarchical $FeWO_4$ Microcrystals: Solvothermal Synthesis and Their Photocatalytic and Magnetic Properties. *Inorg. Chem.* **2009**, *48*, 1082–1090.

(7) Bo Hu, B.; Wu, L. H.; Liu, S. J.; Yao, H. B.; Shi, H. Y.; Li, G. P.; Yu, S. H. Microwave-assisted Synthesis of Silver Indium Tungsten Oxide Mesocrystals and their Selective Photocatalytic Properties. *Chem. Commun.* **2010**, *46*, 2277–2279.

(8) Zhao, D.; Chen, C.; Wang, Y.; Ji, H.; Ma, W.; Zang, L.; Zhao, J. Surface Modification of TiO_2 by Phosphate: Effect on Photocatalytic Activity and Mechanism Implication. *J. Phys. Chem. C* **2008**, *112*, 5993–6001.

(9) Mohapatra, P.; Parida, K. M. Photocatalytic Activity of Sulfate Modified Titania 3: Decolorization of Methylene Blue in Aqueous Solution. *J. Mol. Catal. A* **2006**, *258*, 118–123.

(10) Kudo, A.; Omori, K.; Kato, H. A Novel Aqueous Process for Preparation of Crystal Form-Controlled and Highly Crystalline $BiVO_4$ Powder from Layered Vanadates at Room Temperature and Its Photocatalytic and Photophysical Properties. *J. Am. Chem. Soc.* **1999**, *121*, 11459–11467.

(11) Tang, J. W.; Zou, Z. G.; Ye, J. H. Efficient Photocatalytic Decomposition of Organic Contaminants over $CaBi_2O_4$ under Visible-Light Irradiation. *Angew. Chem., Int. Ed.* **2004**, *43*, 4463–4466.

(12) Fu, H.; Pan, C.; Yao, W.; Zhu, Y. Visible-Light-Induced Degradation of Rhodamine B by Nanosized Bi_2WO_6. *J. Phys. Chem. B* **2005**, *109*, 22432–22439.

(13) Zhu, S.; Xu, T.; Fu, H.; Zhao, J.; Zhu, Y. Synergetic Effect of Bi_2WO_6 Photocatalyst with C_{60} and Enhanced Photoactivity under Visible Irradiation. *Environ. Sci. Technol.* **2007**, *41*, 6234–6239.

(14) Fu, H.; Zhang, S.; Xu, T.; Zhu, Y.; Chen, J. Photocatalytic Degradation of RhB by Fluorinated Bi_2WO_6 and Distributions of the Intermediate Products. *Environ. Sci. Technol.* **2008**, *42*, 2085–2091.

(15) Zhang, L.; Wang, Y.; Cheng, H.; Yao, W.; Zhu, Y. Synthesis of Porous Bi_2WO_6 Thin Films as Efficient Visible Light Active Photocatalysts. *Adv. Mater.* **2009**, *21*, 1286–1290.

(16) Zhang, L.; Wang, W.; Zhou, L.; Xu, H. Bi_2WO_6 Nano- and Microstructures: Shape Control and Associated Visible-Light-Driven Photocatalytic Activities. *Small* **2007**, *3*, 1618–1625.

(17) Chang, T. S.; Guijia, L.; Shin, Ch. H.; Lee, Y. K.; Yun, S. S. Catalytic Behavior of $BiPO_4$ in the Multicomponent Bismuth Phosphate System on the Propylene Ammoxidation. *Catal. Lett.* **2000**, *68*, 229–234.

(18) Elmoudane, M.; Et-tabirou, M.; Hafid, M. Glass-forming Region in the System Li_3PO_4-$Pb_3(PO_4)_2$-$BiPO_4$ (Li_2O-PbO-Bi_2O_3-P_2O_5) and its Ionic Conductivity. *Mater. Res. Bull.* **2000**, *35*, 279–287.

(19) Hölgye, Z. Separation of Neptunium from Urine by Coprecipitation with $BiPO_4$. *J. Radioanal. Nucl. Chem.* **1998**, *227*, 127–128.

(20) Yu, S. H.; Liu, B.; Mo, M. S.; Huang, J. H.; Liu, X. M.; Qian, Y. T. General Synthesis of Single-Crystal Tungstate Nanorods/Nanowires: A Facile Low Temperature Solution Approach. *Adv. Funct. Mater.* **2003**, *13*, 639–647.

(21) Chen, S. F.; Yu, S. H.; Yu, B.; Ren, L.; Yao, W. T.; Cölfen, H. Solvent Effect on Mineral Modification: Selective Synthesis of Cerium Compounds by a Facile Solution Route. *Chem.—Eur. J.* **2004**, *10*, 218–226.

(22) Lei, L.; Dai, Q. High Performance on the Degradation of Cationic Red X-GRL by Wet Electrocatalytic Oxidation Process. *Ind. Eng. Chem. Res.* **2007**, *46*, 8951–8958.

(23) Zhang, H.; Zong, R. L.; Zhao, J. C.; Zhu, Y. F. Dramatic Visible Photocatalytic Degradation Performances Due to Synergetic Effect of TiO_2 with PANI Environ. *Sci. Technol.* **2008**, *42*, 3803–3807.

(24) Buxton, G. V.; Greenstock, C. L.; Helman, W. P.; Ross, A. B. Critical Review of Rate Constants for Reactions of Hydrated Electrons, Hydrogen atoms and Hydroxyl radicals ($OH\bullet/O^{-}\bullet$) in Aqueous Solution. *J. Phys. Chem. Ref. Data* **1988**, *17*, 513–886.

(25) Yoon, S. H.; Lee, J. H. Oxidation Mechanism of As(III) in the UV/TiO_2 System: Evidence for a Direct Hole Oxidation Mechanism. *Environ. Sci. Technol.* **2005**, *39*, 9695–9701.

(26) Zhang, K. L.; Liu, C. M.; Huang, F. Q.; Zheng, C.; Wang, W. D. Study of the Electronic Structure and Photocatalytic Activity of the BiOCl Photocatalyst. *Appl. Catal., B* **2006**, *68*, 125–129.

(27) Kandiel, T. A.; Feldhoff, A.; Robben, L.; Dillert, R.; Bahnemann, D. W. Tailored Titanium Dioxide Nanomaterials: Anatase Nanoparticles and Brookite Nanorods as Highly Active Photocatalysts. *Chem. Mater.* **2010**, *22*, 2050–2060.

(28) Xu, Y.; Schoonen, M. A. A. The Absolute Energy Positions of Conduction and Valence Bands of Selected Semiconducting Minerals. *Am. Mineral.* **2000**, *85*, 543–556.

(29) Yan, T.; Long, J.; Shi, X.; Wang, D.; Li, Z.; Wang, X. Efficient Photocatalytic Degradation of Volatile Organic Compounds by Porous Indium Hydroxide Nanocrystals. *Environ. Sci. Technol.* **2010**, *44*, 1380–1385.

(30) Sun, M.; Li, D.; Zheng, Y.; Zhang, W.; Shao, Y.; Chen, Y.; Li, W.; Fu, X. Microwave Hydrothermal Synthesis of Calcium Antimony Oxide Hydroxide with High Photocatalytic Activity toward Benzene. *Environ. Sci. Technol.* **2009**, *43*, 7877–7882.

(31) Liu, H.; Cheng, Sh.; Wu, M.; Wu, H.; Zhang, J.; Li, W.; Cao, Ch. Photoelectrocatalytic Degradation of Sulfosalicylic Acid and its Electrochemical Impedance Spectroscopy Investigation. *J. Phys. Chem. A* **2000**, *104*, 7016–7020.

(32) Yun, H. J.; Lee, H.; Joo, J. B.; Kim, W.; Yi, J. The Effect of the Preparation Condition of TiO_2 Colloids on Their Surface Structures. *J. Phys. Chem. C* **2009**, *113*, 3050–3055.

(33) Sato, J.; Kobayashi, H.; Inoue, Y. Photocatalytic Activity for Water Decomposition of Indates with Octahedrally Coordinated d10 Configuration. II. Roles of Geometric and Electronic Structures. *J. Phys. Chem. B* **2003**, *107*, 7970–7975.

(34) Zaghiba, K.; Julien, C. M. Structure and Electrochemistry of $FePO_4 \cdot 2H_2O$ Hydrate. *J. Power Sources* **2005**, *142*, 279–284.

ES101223N